Available online at www.sciencedirect.com
ScienceDirect
Trans. Nonferrous Met. Soc. China 28(2018) 2478−2488
Transactions of Nonferrous Metals Society of China
www.tnmsc.cn

Pretreatment-free Ni−P plating on magnesium alloy at low temperatures

P. SHOGHI, D. SEIFZADEH, M. GHOLIZADEH-GHESHLAGHI, A. HABIBI-YANGJEH

Applied Chemistry Department, University of Mohaghegh Ardabili, Ardabil, Iran

Received 24 January 2018; accepted 7 May 2018

Abstract: Electrochemically promoted electroless plating (EPEP) was used for the application of pretreatment-free Ni−P coating on AM60B magnesium alloy at low temperatures and the obtained coating was characterized by SEM, AFM, EDS and XRD techniques. Compact, uniform, and medium-phosphorus Ni−P coating with mixed crystalline−amorphous microstructure was obtained by applying a cathodic current density of 4 mA/cm^2 at 50 °C. Also, island-like nickel clusters were deposited on the alloy surface under the same plating condition but without applying the cathodic current. In addition, the durability of the magnesium alloy against corrosion was strongly improved after plating via EPEP technique which was revealed by electrochemical examinations in 3.5% NaCl (mass fraction) corrosive electrolyte. The results of the electrochemical examinations were confirmed by microscopic observations. Thickness, microhardness, porosity and adhesive strength of the deposits were also qualified.

Key words: magnesium alloy; corrosion; low-temperature electroless plating; Ni−P coating

1 Introduction

Despite many advantageous properties such as lightmass, high thermal stability, good thermal conductivity and good biocompatibility, practical applicability of magnesium-based alloy parts has been restrained mainly because of their low corrosion resistance [1−5]. Several surface treatment technologies such as laser surface cladding [6], PEO [7,8] and CNT reinforcement [9] have been recently suggested for corrosion resistance enhancement of the magnesium alloys. Owing to a remarkable set of advantageous characteristics, involving notable wear resistance, durability against corrosion, excellent microhardness as well as the solderability, electroless Ni−P coating has been extensively suggested to extend the practical applications of magnesium and its alloys as the lightest structural metal parts [10−16]. The electroless nickel coating is generally applied at temperatures of 80−90 °C since plating rate is significantly reduced by a decrease in temperature [17]. Various unavoidable technical problems involving high-energy consuming, poor process control, short service life, and bath decomposition occurred in the electroless Ni−P bath in the above-mentioned temperature range [18–20]. Several strategies including the addition of various additives (such as accelerators) and ultrasonic wave irradiation have been proposed in order to achieve an adequate plating rate at low temperatures [20,21]. In spite of a positive effect on the plating rate, several side-effects such as complication of the plating process, simultaneous deposition of undesired elements, and worsening of the coating's properties may occur during the application of the above-mentioned strategies [18,22]. The electrochemically promoted electroless plating (EPEP) has recently been proposed by GAO et al [19] as a more interesting method for electroless plating on Ti substrate at low temperatures. The proposed method is essentially based on the application of a small cathodic polarization to the substrate during the electroless deposition. It was found that uniform Ni−P coating with medium-phosphorus concentration and good corrosion protection performance can be applied on Ti substrate at 40−60 °C by using EPEP technique. Moreover, the plating rate of the electroless coating on Ti substrate increased after applying the cathodic current which made the Ni−P plating possible at low temperatures.

It seems that EPEP is the most promising technique for direct deposition of the Ni−P layer onto the electrochemically-reactive Mg-based alloy substrates. As frequently discussed in the literature review, an appropriate surface pretreatment is necessary for the Mg-based alloys to overcome the high electrochemical

Corresponding author: D. SEIFZADEH; Tel: +98-4533514702; Fax: +98-4533514701; E-mail: seifzadeh@uma.ac.ir, dseyfzadeh@yahoo.com
DOI: 10.1016/S1003-6326(18)64894-0

reactivity of the surface as the main challenge of the electroless coating process. The traditional surface pretreatment includes pickling in HNO_3−CrO_3 and then activating in HF solutions. Also, several eco-friendly pretreatments before the electroless deposition for the Mg-based alloys have been suggested due to toxicity and corrosivity of CrO_3 and HF, respectively [23−30]. The application of the cathodic polarization during EPEP process decreases the electrochemical reactivity of the magnesium alloy and hence, the electroless plating will be possible at low temperatures without any especial pretreatment in completely environmentally-friendly condition.

Therefore, ability of EPEP technique to apply the Ni−P deposit on AM60B alloy substrate at low temperatures without any especial pretreatment was evaluated in this investigation. Also, the applied coating was fully studied from the morphological, topographical, compositional, and microstructural points of views by SEM, AFM, EDS, and XRD techniques, respectively. The corrosion protection capacity of the resultant Ni−P layer was also examined by executing accelerated corrosion examinations in 3.5% NaCl (mass fraction) corrosion testing electrolyte using EIS (electrochemical impedance spectroscopy) and PDP (potentiodynamic polarization) techniques. Moreover, the microhardness, porosity and adhesive strength of the Ni−P deposit were estimated by appropriate experiments.

2 Experimental

2.1 Electroless plating process

AM60B alloy bar with an elemental composition of 6.33% Al, 0.24% Mn, 0.68% Zn, and magnesium-reminder (mass fraction), which was supplied from Nanjing Welbow Metals Co., Ltd., was cut into small pieces (70 mm × 10 mm × 4 mm) for the electroless plating. Prior to the final EPEP process, AM60B specimens were consecutively abraded with different grades of sand papers (120, 400, 1000 and 2000), and degreased by an alkaline solution (40 g/L NaOH and 10 g/L $Na_3PO_4{\cdot}12H_2O$) at 60 °C for 15 min, and then etched in 50 mL/L HNO_3 (Royalex, 69%−71%) solution for about 30 s. At the end, EPEP technique was used for the application of the Ni−P coating using a typical sulfate plating solution. The samples were thoroughly washed by deionized water between different steps. The bath composition and operation condition of the plating process are shown in Table 1.

The plating process was carried out in 500 mL plating solution. Two different Pt sheets (1 cm^2) were used as auxillary electrodes (AE) on front and back sides of the magnesium alloy substrate (as working electrode, WE) so that the distance between each AE and WE was about 5 cm. WE and AE were connected to the negative and positive terminals of a DC power supply, respectively, and the impressed current was controlled by a digital ammeter. Also, a separate alloy sample was plated at the same plating bath and operation condition but without applying any cathodic polarization in order to clarify the role of the impressed current.

Table 1 Chemical compositions and operation conditions of plating bath in EPEP process

Chemical agent	Concentration/ ($g{\cdot}L^{-1}$)	Operation condition
$NiSO_4{\cdot}6H_2O$ (Rankem, 97%)	15	Temperature: (50±2) °C; Plating time: 2 h; Impressed cathodic current density: 4 mA/cm^2
$NaH_2PO_2{\cdot}H_2O$ (Merck, 99%)	14	
CH_3COONa (Merck, 99.5%)	13	
NH_4HF_2 (Merck, 98%)	8	
HF (Merck, 40%)	12*	
NH_4OH (Royalex, 30%)	For adjusting pH to 6.4	

* mL/L

2.2 Surface analysis

A SEM device (Carl-Zeiss Model LEO VP 1430) was utilized in order to analyze the Ni−P deposit from a morphological point of view. A backscattered electron detector was used to obtain surface morphological images at low (600×) and high (20000×) magnifications and the analyses were performed under high vacuum condition by using an accelerating voltage of 15 kV without gold plating. Also, the cross-section area of the electroless coating was morphologically studied by SEM. For this purpose, the plated alloy sample was carefully cut and then, the cross-section area of the coating was mildly polished with SiC sand papers (1000 and 2000 grits). Next, the sample was degreased with ethanol and its cross-sectional SEM image was taken at 450× magnification without any gold plating.

The surface roughness of the Ni−P deposit was also estimated by obtaining its topographic image using the AFM (Nano Ink Dpn 5000) instrument. Also, the elemental composition and microstructure of the resultant electroless layer were studied through recording EDS (RÖNTEC GmbH Germany) spectrum and XRD (Philips Xpert diffractometer using a Cu K_α radiation source and λ=0.154 nm) pattern, respectively.

2.3 Corrosion behavior

Improvement in durability of AM60B alloy against corrosion after the Ni−P deposition was studied by two

traditional corrosion monitoring techniques (PDP and EIS) in 3.5% NaCl (mass fraction) electrolyte at room temperature (≈24 °C). A computer-controlled potentiostat−galvanostat device (μAutolam3) connected to a typical three-electrode cell consisting of the alloy specimen (masked with multi-layer epoxy resin to leave an exposed area of 1 cm^2) as WE, a Pt plate electrode (1 cm^2) as AE, and a Ag/AgCl electrode (filled by saturated KCl) as reference electrode (RE) was employed to perform the corrosion tests. First of all, the samples were kept in the corrosive media for about 15 min in order to establish a steady-state open circuit potential (OCP) and then, EIS and PDP examinations were performed, consecutively. For EIS measurements, an alternative voltage of 20 mV was impressed around the OCP of WE through the entire frequency band between 10 kHz to 10 mHz. In each EIS experiment, 42 different data points were recorded and the experimental results were analyzed using Zview2 equivalent circuit fitting software. The PDP tests were immediately executed after EIS measurements by scanning the potential at a sweeping speed of 1 mV/s from the negative to positive direction. The data obtained by the corrosion monitoring methods were also approved by the microscopic observations after PDP test. For this purpose, the tested samples were immediately removed from the corrosive solution after PDP tests, washed with deionized water, dried with compressed warm air, and finally morphologically analyzed by SEM.

2.4 Thermal shock test

Thermal shock experiment was fulfilled in accordance with ASTM B733–04 to examine the adhesion between AM60B alloy surface and the Ni−P layer. For this purpose, the coated sample was kept in a pre-heated digital furnace at 200 °C for about 10 min and then quickly quenched in cool water (≈ 20 °C). Then, the sample was removed from the water and dried by compressed warm air. Next, the sample was carefully checked to detect possible bubbles, cracks, peeling, warping, and flaking as evidence of poor adhesion.

2.5 Microhardness measurement

A Shimadzu HMV−G20 device with diamond indenter was utilized to measure the microhardness of the Ni−P deposit according to ASTM B578. The measurements were repeated four times using a load of 100 g and a dwell time of 10 s and the mean microhardness value was calculated.

2.6 Porosity test

The porosity of the Ni–P deposit on AM60B alloy is a very important parameter due to the large electrochemical potential gap between Ni coating and AM60B substrate which strongly increases the risk of the galvanic corrosion in the porous area. So, the porosity of the applied electroless coating was studied according to the experimental procedure which was previously described elsewhere [14]. To perform the porosity test, a piece of filter paper with a surface area of 1 cm^2 was immersed in a special aqueous solution (containing 10 g/L NaCl, 10 g/L ethanol and 0.1 g/L phenolphthalein). Afterwards, the filter paper was pasted on the coating surface immediately. After 10 min, the filter paper was removed from the surface and the porosity was estimated by dividing the number of probable red points on the filter paper to the total contact area.

3 Results and discussion

3.1 Surface and mechanistic analyses

The micromorphological features of the alloy surface after 2 h plating via EPEP technique were studied by SEM at low (Fig. 1(a)) and high (Fig. 1(b)) magnifications.

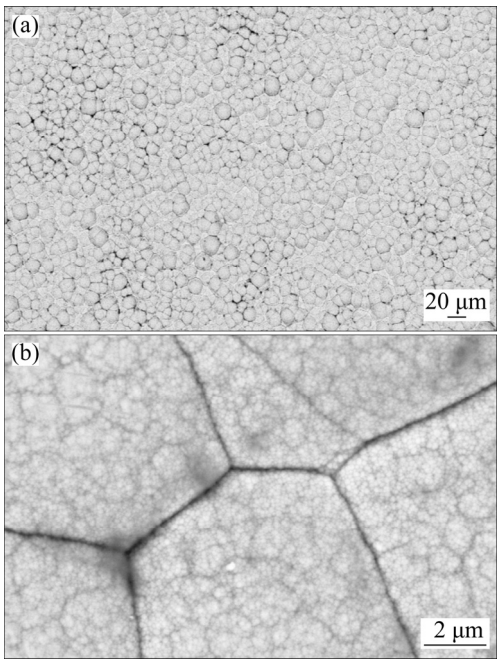

Fig. 1 Surface morphology of Ni−P coating via EPEP technique at low (a) and high (b) magnifications

The microscopic appearance indicated the formation of even, defect-free, and cauliflower-like nodular Ni−P deposit with uniform nodule-size distribution. The high-magnification SEM observation (Fig. 1(b)) revealed that the spherical nodular structure of the electroless layer was highly compact so that there was no obvious inter-granular space between the grains.

The topographic image (Fig. 2) of the resultant Ni−P deposit was also obtained by AFM method to estimate the roughness of the coating.

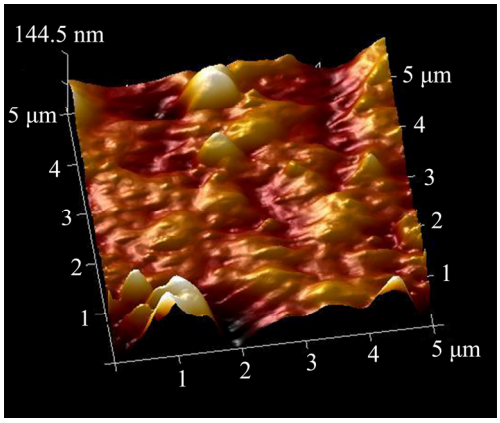

Fig. 2 Topographic image of sample coated via EPEP technique

The average roughness (R_a) and root mean square roughness (R_q) of the Ni−P deposit in the analyzed area (25 μm^2) were estimated to be 19.4 and 29.0 nm, respectively, which indicated the uniformity of the applied coating.

EDS analysis from three different locations (typical EDS spectrum is illustrated in Fig. 3) shows that the coating is composed of 92.12% Ni and 7.88% P, which is in consistent with its typical nodular structure [31].

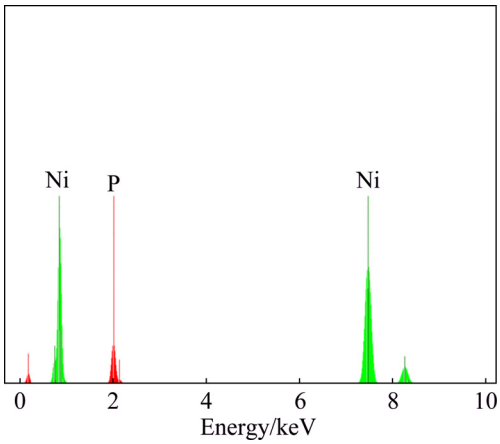

Fig. 3 EDS spectrum taken from surface of electroless deposit achieved via EPEP technique

Moreover, a broad characteristic peak for Ni (111) plane was detected in the XRD pattern of the applied Ni−P layer (Fig. 4). This result means that the coating presents a mixed amorphous-crystalline microstructure due to low degree of crystallization, which is in agreement with the result of EDS analysis which reveals the moderate P content of the coating [32]. The cross-sectional zone of the coated sample was also investigated via SEM technique to characterize the morphology of the coating/substrate interface (Fig. 5).

It is clear that there is good mechanical interlocking between the plated layer and AM60B substrate, and thickness of the coating is about 21 μm. The observed

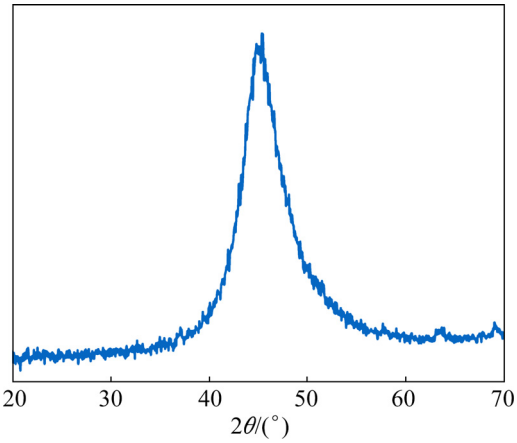

Fig. 4 XRD pattern of Ni−P deposit achieved via EPEP technique

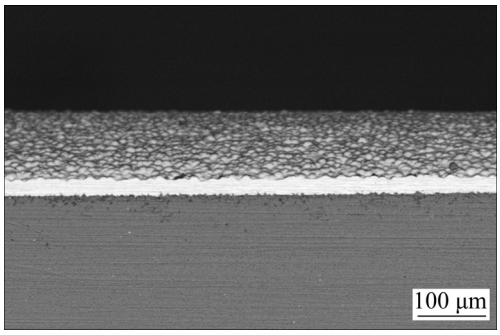

Fig. 5 SEM image of cross-section of Ni−P deposit plated by EPEP technique

plating rate (10.5 μm/h) can be considered as an ideal value at 50 °C compared to the plating rate values previously reported for the high-temperature electroless deposition of the Mg-based alloy substrates [33]. The above-mentioned results clearly show that EPEP is a simple and successful approach for the electroless nickel plating on AM60B substrate at sufficiently low temperature without any especial pretreatment. It is well known that rapid oxidation of the untreated Mg-based substrate in the electroless bath (in competition with the electroless process) is the most significant problem in direct Ni−P deposition. The applied cathodic polarization inhibited the electrochemical oxidation of AM60B magnesium alloy substrate and therefore, provided suitable condition for the pretreatment-free Ni−P coating. This issue can be briefly discussed using the theory of the electrochemical kinetics. The main mechanism for the corrosion of the magnesium alloy in the brine corrosive media can be expressed as follows:

$$Mg = Mg^{2+} + 2e \quad (1)$$

$$2H_2O + O_2 + 4e = 4OH^- \quad (2)$$

In steady state corrosion condition, the rates of both the cathodic and anodic processes are equal. Also, the

rate of the overall corrosion reaction is determined by the slowest or rate determining step. On the other hand, it is well known that the rate constant of the heterogeneous electrochemical process depends on the potential. The potential dependence of the rate constant for the above-mentioned anodic and cathodic reactions can be expressed as follows [34]:

$$K_a = K_a^o \exp\left[\frac{\alpha_a nF}{RT}(\varphi - \varphi^{o'})\right] \quad (3)$$

$$K_c = K_c^o \exp\left[\frac{-\alpha_c nF}{RT}(\varphi - \varphi^{o'})\right] \quad (4)$$

where K_a and K_c are the rate constants of the magnesium oxidation and water reduction reactions, respectively. Also, n, T, F and R are the electron transfer number, thermodynamic temperature, Faraday constant and mole gas constant, respectively. In addition, φ and $\varphi^{o'}$ are the potential and formal potential of the electrode, respectively. Also, α_a and α_c are electron transfer coefficients of the oxidation and reduction reactions, respectively. Finally, K_a^o and K_c^o are the standard rate constants of magnesium oxidation and water reduction reactions, respectively. Based on the above mentioned equations, it may be easily concluded that the application of any cathodic (negative) potential to the electrode decreases the rate constant and hence the rate of the magnesium oxidation reaction. In fact, the application of the negative potential to the electrode increases the activation energy of the anodic process which leads to decreasing the rate. So, one of the main challenges of the Ni–P deposition on the magnesium-based substrate was solved by the application of the cathodic polarization.

Also, the electroless coating was performed under the same operating condition but without applying the cathodic polarization to the substrate in order to clarify the role of the impressed cathodic current. Figure 6 shows the surface morphological features of the untreated alloy specimen after plating in the low-temperature electroless bath without applying the cathodic current at two different magnifications.

The microscopic observation revealed that the alloy substrate was strongly damaged by the corrosion process and there was no continuous electroless film on the alloy surface. As a replacement, some island-like and bright structures were observed on the alloy surface. Also, the formation of some discrete cauliflower-like Ni deposits in the bright zones was revealed by the high-magnification SEM observation (Fig. 6(b)). These nickel structures were more probably created as a result of electrochemical replacement reaction between Mg atoms in the substrate and free Ni^{2+} ions in the plating bath ($Ni^{2+}+Mg=Ni+Mg^{2+}$). However, the created Ni nuclei were unable to grow in horizontal and vertical

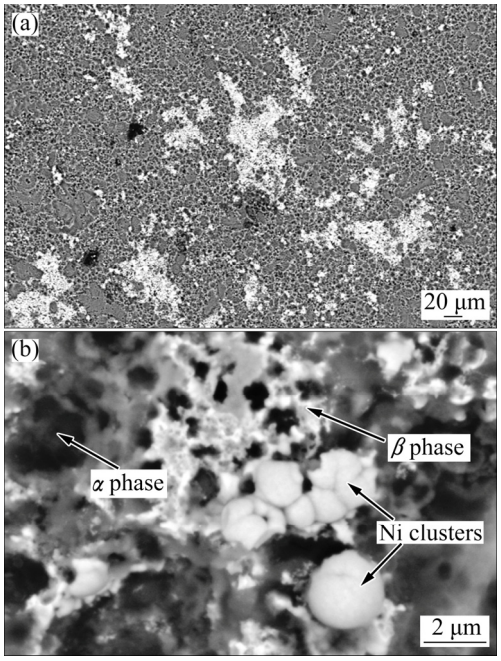

Fig. 6 SEM images of untreated AM60B alloy substrate after immersion in Ni−P plating bath without applying cathodic current at low (a) and high (b) magnifications

directions to cover the alloy substrate because the plating process is essentially impossible at low temperature without applying the cathodic current. This situation promotes the dissolution of the active α-phase zones (magnesium-rich phase) [35] because of intense galvanic effect between the locally-deposited Ni particles and the magnesium alloy. Selective and rapid dissolution of the α-phase regions caused the formation of loose β-phase ($Mg_{17}Al_{12}$) structures near the locally-deposited Ni clusters which can be easily observed by the high-magnification SEM image (Fig. 6(b)). Based on the above-mentioned results, the traditional electroless plating of the magnesium-based substrate is essentially impossible at 50 °C. Also, it can be concluded that the applied cathodic potential has great effect on the rate of the Ni−P plating. This fact may be explained via the electrochemical kinetics theory which was described above. The following mechanisms can be regarded for the electroless Ni–P deposition [12]:

$$Ni^{2+}+2e=Ni \quad (5)$$

$$2H_2PO_2^- + 2H_2O = 2H_2PO_3^- + 2H^+ + H_2 + 2e \quad (6)$$

$$2H_2PO_2^- + 6H^+ + 4H_2O + 12e = 2P + 5H_2 + 8OH^- \quad (7)$$

According to Eq. (4), the rate constant of a heterogeneous cathodic reaction increases by applying negative potential to the electrode. Therefore, it seems that the applied cathodic current increases the rate constant of the Ni^{2+} reduction process by decreasing its activation energy.

On the other hand, it is necessary to use the complexing agents in the electroless bath to control the free Ni^{2+} ions concentration in the plating solution which has negative effect on the plating rate. Hence, the plating rate promotion under the cathodic polarization may be related to the acceleration of electrical migration of Ni^{2+} ions towards the magnesium alloy substrate.

The applied cathodic polarization may cause direct reduction of Ni^{2+} ions on the alloy surface. To investigate this issue, the plating was carried out in the same operation condition under the cathodic polarization but without adding reducing agent ($NaH_2PO_2·H_2O$) to the plating bath. After this examination, no plating was observed either by the visual observation or gravimetric measurement. This fact clearly shows that the applied small cathodic potential is unable to directly reduce the Ni^{2+} ions.

3.2 Microhardness measurement

The mean microhardness of the Ni−P deposit (achieved via EPEP technique) was evaluated by performing four different tests. The average value was about $HV_{0.1}$ 624 which is far from the microhardness of AM60B magnesium alloy ($HV_{0.1}$ 83). The microhardness of a Ni−P coating depends on the plating condition. However, the obtained microhardness value can be considered as a good result compared with the results which were previously obtained in other investigations [36−38].

3.3 Thermal shock examination

The adhesive strength between the deposited layer and AM60B alloy is another important factor that should be evaluated. As it is obvious from the microscopic appearance of the cross-sectional area (Fig. 5) that mechanical interlocking across the interface between the Ni−P deposit and AM60B alloy is strong due to etching of the substrate in acid pickling step before the final electroless process (indicating good coating/substrate adhesion). However, the thermal shock examination was also performed in accordance with the experimental procedure that was described in Section 2.4 to confirm SEM result about the adhesion. Figure 7 presents the visual image that was recorded by a digital camera from the coated surface after 20-cycle thermal stress testing. It is obvious that there are no cracks, blistering, peeling, flaking or any other evidence of weak adhesion at the coating/substrate interface. This means that the adherent electroless coating can be deposited on AM60B alloy substrate via EPEP technique.

3.4 Porosity

The porosity test was performed to reveal the pore-free nature of the deposited electroless layer which is critical factor for the cathodic nickel deposit on the anodic magnesium-based substrate. It is clear from Fig. 8 that there are no red points on the removed filter paper, indicating that the Ni−P deposit is completely pore-free. It should be explained that suitable condition for the penetration of the aqueous test solution towards the magnesium alloy substrate will be provided through the possible pores in the coating. In this situation, the red points will appear on the phenolphthalein-containing filter paper due to local alkalinity arising from the rapid reduction of water ($2H_2O+O_2+4e \rightarrow 4OH^-$) as the main cathodic corrosion process. The above-mentioned results clearly show the efficiency of EPEP technique to apply high-quality Ni−P layer on AM60B substrate.

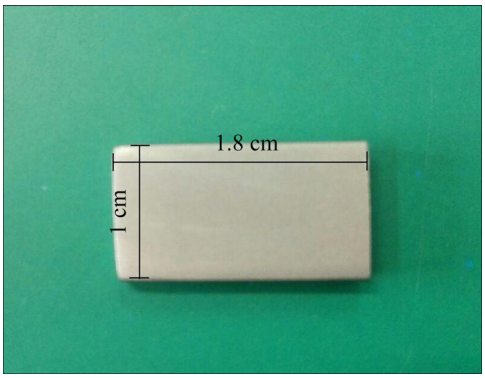

Fig. 7 Visual image of Ni−P coated alloy sample after 20-cycle thermal shock test

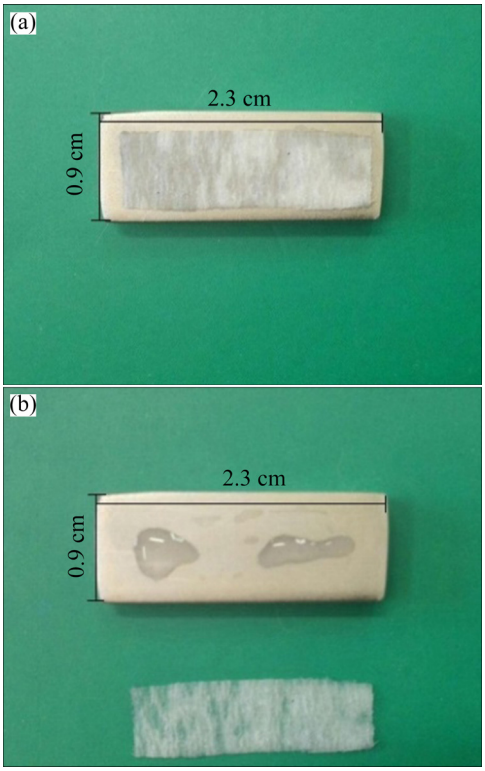

Fig. 8 Visual images corresponding to porosity tests after pasting filter paper (a) and after removing filter paper (b)

3.5 Corrosion behavior

As a modern corrosion monitoring method, EIS, was used for analyzing the protection characteristics of the applied coating. First of all, the impedance response of AM60B bare specimen in the corrosive electrolyte was recorded as Nyquist (Fig. 9(a)), Bode modulus (Fig. 9(b)), and phase Bode (Fig. 9(c)) plots.

An obvious capacitive arc was detected in the Nyquist plot of the bare alloy sample which was followed by a scattered inductive semicircle at the lowest measured frequencies. The observed EIS response is typical for the magnesium alloys in the brine corrosive solutions and was previously discussed by many researchers. The capacitive arc at high measured frequencies is corresponding to the electron transfer process across the electrode/electrolyte interface or to oxide/hydroxide layers on the metal surface and its diameter is inversely related to the corrosion rate. Also, the inductive arc at low frequencies is associated with adsorbed species on the electrode or pitting corrosion [39,40]. The impedance responses of the plated specimens are also illustrated in Fig. 10. Also, the OCP values of the Ni−P coating were continuously recorded before EIS test to confirm the electrode stability (Fig. 10(d)).

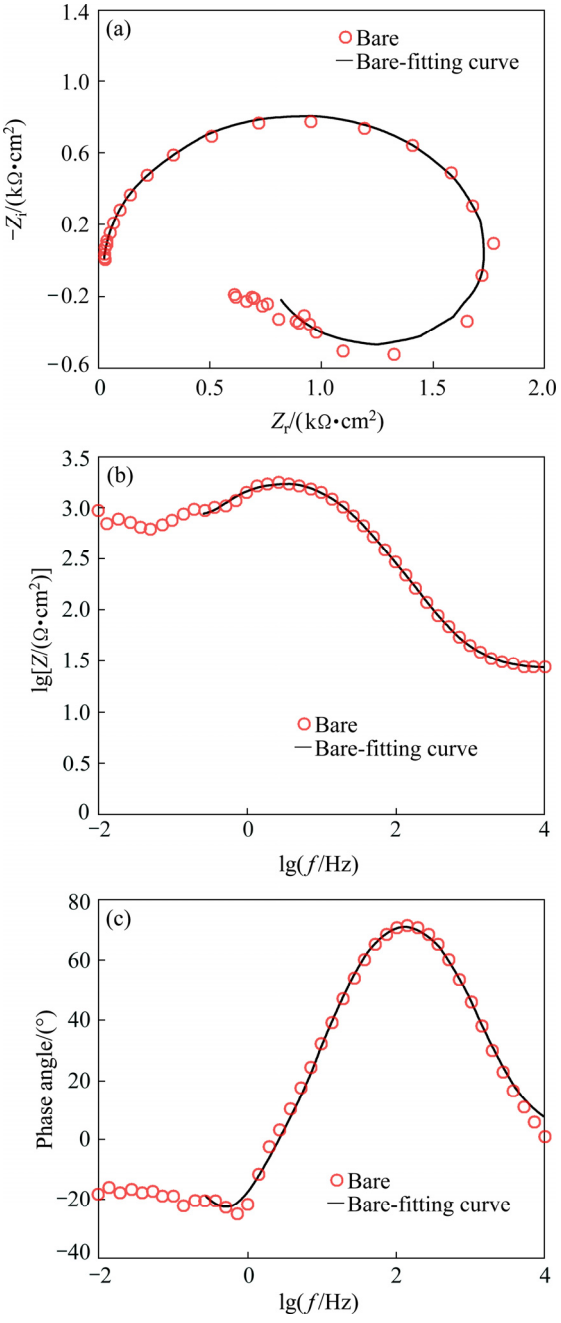

Fig. 9 Impedance response of AM60B bare alloy in 3.5% NaCl electrolyte as Nyquist (a), Bode modulus (b) and phase Bode (c) plots

It is clear that one capacitive arc was only observed for the coated samples which can be ascribed to the charge transfer phenomenon. The alloy sample coated via EPEP technique showed a large and depressed capacitive semicircle with a diameter much higher than that observed for the bare alloy, indicating corrosion resistance improvement. Oppositely, a very small capacitive semicircle was recorded for the sample plated without applying the cathodic current even very smaller than that obtained for the bare alloy sample. This result is more probably related to the fact that the sample was severely corroded in the plating solution during the unsuccessful plating process at low temperatures without applying the cathodic current because of serious galvanic effect between the locally-deposited Ni−P clusters and α-phase of the magnesium alloy. Also, the mentioned sample was strongly corroded in the corrosive solution by the galvanic effect during initial hold time before starting the corrosion tests. The strong corrosion process caused the dissolution of the partially-protective oxide/hydroxide film on the alloy surface. Also, effective surface area of the mentioned sample was increased due to serious corrosion. These factors decreased its corrosion resistance compared with the bare alloy sample.

EIS response for the bare and Ni−P deposited alloy substrates was fitted by two different equivalent circuits illustrated in Figs. 11(a) [39] and (b) [27], respectively.

In the first circuit model (Fig. 11(a)), R_s and R_{ct} are inserted to describe the resistive behavior of the electrolyte and charge transfer process, respectively, while CPE_{dl} is a constant phase element (CPE) which is utilized to model non-ideal double layer capacitor. To model the inductive behavior at lowest frequencies, resistance R_L and inductor L elements were additionally added to the circuit [39]. Also, in the second electrical model, R_s, R_{ct}, and CPE_{dl} are corresponding to the resistances of the testing electrolyte, charge transfer resistance, and double layer capacitor, respectively [27]. The quantitative results are collected in Table 2, which revealed meaningful enhancement in the resistance of

AM60B alloy against corrosion after applying the Ni−P coating via EPEP technique. Also, very low corrosion resistance was calculated for the alloy sample plated without applying the cathodic current.

The corrosion behaviors of AM60B sample without and with applying the Ni−P coatings were also analyzed by the PDP method. Figure 12 demonstrates the corresponding PDP curves in the corrosion testing

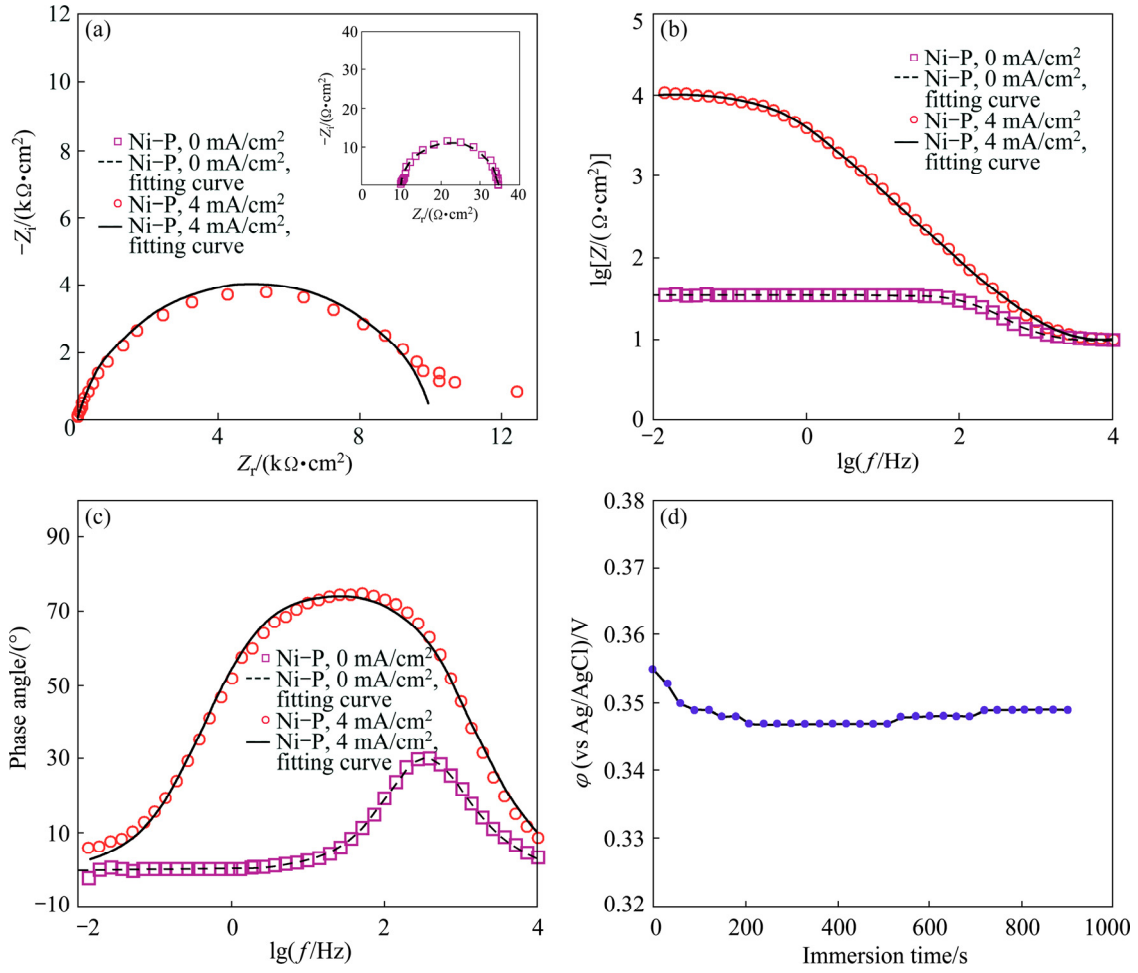

Fig. 10 Impedance response of Ni−P coated alloy samples in 3.5% NaCl electrolyte as Nyquist (a), Bode modulus (b), phase Bode (c) plots, and OCP changes versus immersion time plot (d)

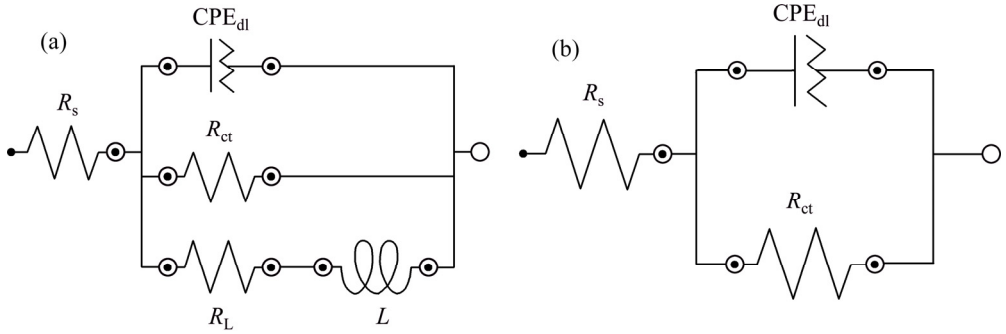

Fig. 11 Appropriate equivalent circuits for fitting EIS response of bare (a) and Ni−P coated (b) alloy substrates

Table 2 Quantitative EIS results for unplated and plated specimens in corrosion testing electrolyte

Sample	R_{ct}/(kΩ·cm^2)	CPE$_{dl}$/(μs^n·Ω^{-1}·cm^{-2})	n	R_L/(kΩ·cm^2)	L/(H·cm^{-2})	Chi-squared
Bare	1.78±0.03	7.96±0.33	0.944±0.006	1.28±0.06	573.9±27.5	0.0049
Ni−P (EPEP)	10.06±0.10	42.24±0.58	0.861±0.002	–	–	0.0033
Ni−P (without applying current)	0.02±0.00	55.99±0.15	0.936±0.004	–	–	0.0025

solution while the related polarization parameters including b_c (cathodic Tafel slope), φ_{corr} (corrosion potential), and J_{corr} (corrosion current density) were given in Table 3. It should be noted that PDP parameters were extracted via cathodic Tafel extrapolation technique which has been confirmed as reliable analysis method to accurately extract the quantitative corrosion parameters of the magnesium alloys [41].

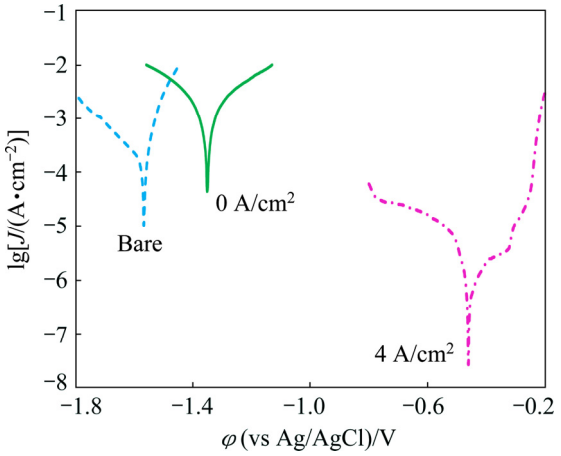

Fig. 12 PDP curves of bare and Ni−P plated alloy substrates

A significant ennoblement in the corrosion potential of the alloy sample can be seen after application of the Ni−P deposit via EPEP technique. The observed noble corrosion potential clearly indicates the compactness and pore-free nature of the electroless film which effectively hinders the penetration of the aggressive species towards the substrate. It should be explained that the electrolyte penetration through the possible pores or defects causes the formation of strong galvanic effect between Ni coating and Mg substrate due to large deference between their electrochemical potentials. The corrosion potential of nickel coating shifts towards negative direction in such a situation and simultaneously, Mg substrate suffers from serious corrosion at the bottom of the defects. These observations were not seen in this study and the corrosion potential of the Ni−P coating was stable, which confirmed its compactness [42]. In addition, pseudo-passivation behavior was seen in anodic branch of the polarization curve after the Ni−P coating via EPEP technique, indicating its good corrosion protection capacity [12].

Also, J_{corr} value of AM60B bare sample was decreased by 97.7% after the electroless deposition through EPEP technique at low temperatures, which obviously demonstrated the effectiveness of the resultant Ni−P coating from the corrosion protection point of view. In addition, φ_{corr} value of the alloy sample shifted only about 200 mV towards the positive direction after unsuccessful electroless plating without applying the cathodic potential at low temperatures. This sample also showed very high corrosion current density so that the corresponding J_{corr} value was about 10 times higher than that of the bare alloy sample (Table 3). These results are in good consistent with those obtained from the EIS testing.

Moreover, the anticorrosion effectiveness of the Ni−P coatings was microscopically evaluated after PDP tests by SEM. Figure 13 illustrates the morphological changes of the bare and Ni−P coated (with and without applying the cathodic current) after PDP experiments in 3.5% NaCl electrolyte. The bare alloy was seriously suffered from the corrosion under the applied anodic

Table 3 PDP results for unplated and plated alloy specimens in corrosion testing electrolyte

Sample	φ_{corr} (vs Ag/AgCl)/V	$-b_c$/(mV·dec^{-1})	J_{corr}/(μA·cm^{-2})
Bare	−1.568	182	151.8
Ni−P (EPEP)	−0.460	172	3.5
Ni−P (without applying current)	−1.352	135	1666.5

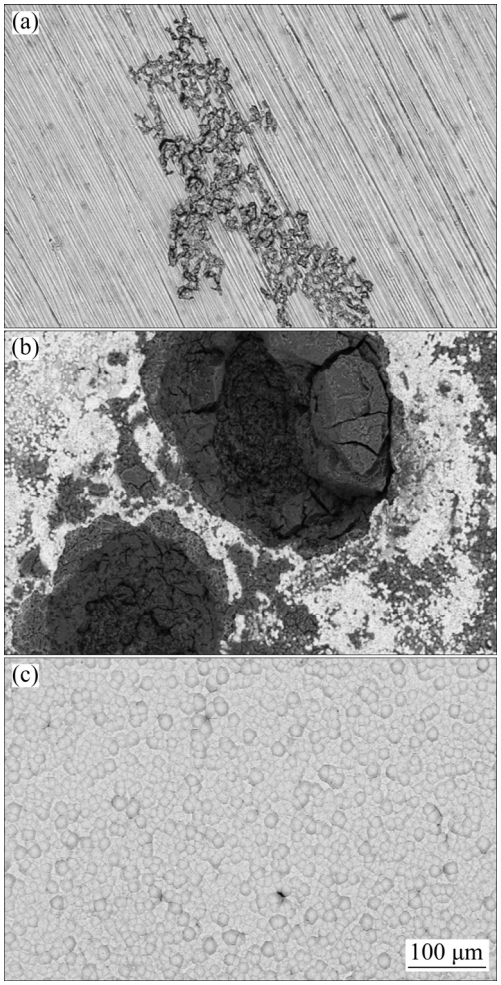

Fig. 13 Surface morphologies of bare (a) and Ni−P coated samples without (b) and with (c) applying cathodic current after PDP testing

polarization during PDP testing as can be seen from Fig. 13(a). Also, the alloy sample which was plated without applying the cathodic current showed very sever corrosion attacks especially in the α-phase area because of the formation of very strong galvanic effect in the plating and corrosive solutions (Fig. 13(b)); but there was no obvious localized corrosion damage on the surface of the sample coated by EPEP technique (Fig. 13(c)). In fact, the results of the electrochemical examinations were confirmed by the microscopic observations.

4 Conclusions

1) EPEP technique was proven to be a promising technique for pretreatment-free Ni−P deposition onto AM60B alloy at low temperatures.

2) SEM, AFM, EDS, and XRD examinations confirmed the formation of compact, nodular, uniform, medium-phosphorus, and mixed crystalline-amorphous Ni−P coating on AM60B alloy by applying 4 mA/cm^2 cathodic current at 50 °C without any especial pretreatment.

3) The pretreatment-free Ni−P coating cannot be achieved onto AM60B substrate at 50 °C without applying the cathodic current and island-like Ni clusters can be only deposited in this situation.

4) The corrosion resistance of the magnesium alloy in 3.5% NaCl corrosive medium was strongly improved by applying the Ni−P deposit via EPEP technique. Oppositely, the corrosion resistance was reduced relatively to the bare substrate after pretreatment-free and low-temperature Ni−P plating without applying the cathodic current.

5) The microhardness of AM60B substrate was meaningfully increased by the Ni−P deposition via EPEP technique.

6) The results of the thermal shock and porosity tests showed that nonporous and adhesive Ni−P deposit can be achieved on AM60B magnesium alloy via EPEP technique.

References

[1] SUN Y H, WANG R C, PENG C Q, FENG Y, YAN M. Corrosion behavior and surface treatment of superlight Mg−Li alloys [J]. Transactions of Nonferrous Metals Society of China, 2017, 27: 1455−1475.

[2] CUI L Y, ZENG R C, GUAN S K, QI W C, ZHANG F, LI S Q, HAN E H. Degradation mechanism of micro-arc oxidation coatings on biodegradable Mg−Ca alloys: The influence of porosity [J]. Journal of Alloys and Compounds, 2017, 695: 2464−2476.

[3] PHUONG N V, GUPTA M, MOON S. Enhanced corrosion performance of magnesium phosphate conversion coating on AZ31 magnesium alloy [J]. Transactions of Nonferrous Metals Society of China, 2017, 27: 1087−1095.

[4] CUI L Y, GAO S D, LI P P, ZENG R C, ZHANG F, LI S Q, HAN E H. Corrosion resistance of a self-healing micro-arc oxidation/ polymethyltrimethoxysilane composite coating on magnesium alloy AZ31 [J]. Corrosion Science, 2017, 118: 84−95.

[5] WANG C, WU L, XUE F, MA R, ETIM I, HAO X, DONG J, KE W. Electrochemical noise analysis on the pit corrosion susceptibility of biodegradable AZ31 magnesium alloy in four types of simulated body solutions [J]. Journal of Materials Science & Technology, 2018, 34: 1876−1884.

[6] ZHANG X L, ZHANG K M, ZOU J X. Microstructures and properties in surface layers of Mg−6Zn−1Ca magnesium alloy laser-clad with Al−Si powders [J]. Transactions of Nonferrous Metals Society of China, 2018, 28: 96−102.

[7] PEZZATO L, ANGELINI V, BRUNELLI K, MARTINI C, DABALA M. Tribological and corrosion behavior of PEO coatings with graphite nanoparticles on AZ91 and AZ80 magnesium alloys [J]. Transactions of Nonferrous Metal Society of China, 2018, 28: 259−272.

[8] ZENG R, CUI L, JIANG K, LIU R, ZHAO B, ZHENG Y. In vitro corrosion and cytocompatibility of a microarc oxidation coating and poly(*L*-lactic acid) composite coating on Mg−1Li−1Ca alloy for orthopaedic implants [J]. ACS Applied Materials & Interfaces, 2016, 8: 10014−10028.

[9] YUAN Q H, FU D M, ZENG X S, LIU Y. Fabrication of carbon nanotube reinforced AZ91D composite with superior mechanical properties [J]. Transactions of Nonferrous Metals Society of China 2017, 27: 1716−1724.

[10] CALDERON J A, JIMENEZ J P, ZULETA A A. Improvement of the erosion-corrosion resistance of magnesium by electroless Ni−P/$Ni(OH)_2$–ceramic nanoparticle composite coatings [J]. Surface and Coatings Technology, 2016, 304: 167−178.

[11] RAJABALIZADEH Z, SEIFZADEH D. Strontium phosphate conversion coating as an economical and environmentally-friendly pretreatment for electroless plating on AM60B magnesium alloy [J]. Surface and Coatings Technology, 2016, 304: 450−458.

[12] RAJABALIZADEH Z, SEIFZADEH D. Application of electroless Ni−P coating on magnesium alloy via CrO_3/HF free titanate pretreatment [J]. Applied Surface Science, 2017, 422: 696−709.

[13] LIU W, XU D D, DUAN X Y, ZHAO G S, CHANG L M, LI X. Structure and effects of electroless Ni–Sn–P transition layer during acid electroless plating on magnesium alloys [J]. Transactions of Nonferrous Metals Society of China, 2015, 25: 1506−1516.

[14] SEIFZADEH D, KAZEMI MOHSENABADI H, RAJABA-LIZADEH Z. Electroless Ni−P plating on magnesium alloy by innovative, simple and non-toxic oxalate pretreatment and its corrosion protection [J]. RSC Advance, 206, 6: 97241−97252.

[15] ZHANG M, MU S, GUAN Q, LI W, DU J. A high anticorrosive chromium-free conversion coating prepared with an alkaline conversion bath on electroless Ni−P coating [J]. Applied Surface Science, 2015, 349: 108−115.

[16] SADREDDINI S, RAHEMI ARDAKANI S, RASSAEE H. Corrosion behavior and microhardness of Ni−P−SiO_2−Al_2O_3 nano-composite coatings on magnesium alloy [J]. Journal of Materials Engineering and Performance, 2017, 26: 2032−2039.

[17] LIU J, WANG X, TIAN Z, YUAN M, MA X. Effect of copper content on the properties of electroless Ni–Cu–P coatings prepared on magnesium alloys [J]. Applied Surface Science, 2015, 356: 289−293.

[18] KANG R, PENG Z, LIU B, WANG D, LIANG J. A protocol for fast electroless Ni−P on Al alloy at medium-low temperature accelerated by hierarchically structured Cu immersion layer [J]. Surface and Coatings Technology, 2017, 309: 67−74.

[19] GAO C, DAI L, MENG W, HE Z, WANG L. Electrochemically promoted electroless nickel–phosphorous plating on titanium substrate [J]. Applied Surface Science, 2017, 392: 912−919.

[20] MAO G. Fast electroless Ni−P coating on AM60 magnesium alloy at low bath temperature [J]. Advanced Materials Research, 2012, 418−420: 756−759.
[21] ZOU Y, ZHANG Z, LIU S, CHEN D, WANG G, WANG Y, ZHANG M, CHEN Y. Ultrasonic-assisted electroless Ni−P plating on dual phase Mg−Li alloy [J]. Journal of Electrochemical Society, 2015, 162: C64−C70.
[22] BASKARAN I, SANKARA NARAYANAN T S N, STEPHEN A. Effect of accelerators and stabilizers on the formation and characteristics of electroless Ni−P deposits [J]. Materials Chemistry and Physics, 2006, 99: 117–126.
[23] YAN D, YU G, HU B, ZHANG J, SONG Z, ZHANG X. An innovative procedure of electroless nickel plating in fluoride-free bath used for AZ91D magnesium alloy [J]. Journal of Alloys and Compounds, 2015, 653: 271−278.
[24] SUN C, GUO X W, WANG S H, GUO J C, DING W J. Homogenization pretreatment and electroless Ni−P plating on AZ91D magnesium alloy [J]. Transactions of Nonferrous Metals Society of China, 2014, 24: 3825−3833.
[25] SONG Z, XIE Z, YU G, HU B, HE X, ZHANG X. A novel palladium-free surface activation process for electroless nickel deposition on micro-arc oxidation film of AZ91D Mg alloy [J]. Journal of Alloys and Compounds, 2015, 623: 274−281.
[26] SEIFZADEH D, RAHIMZADEH HOLLAGH A. Corrosion resistance enhancement of AZ91D magnesium alloy by electroless Ni−Co−P coating and Ni−Co−P−SiO_2 nanocomposite [J]. Journal of Materials Engineering and Performance, 2014, 23: 4109−4121.
[27] SEIFZADEH D, RAJABALIZADEH Z. Environmentally-friendly method for electroless Ni−P plating on magnesium alloy [J]. Surface and Coatings Technology, 2013, 218: 119−126.
[28] FAN X, WANG Y, ZOU B, GU L, HUANG W, CAO X. Preparation and corrosion resistance of MAO/Ni−P composite coat on Mg alloy [J]. Applied Surface Science, 2013, 277: 272−280.
[29] ZULETA A A, CORREA E, CASTANO J G, ECHEVERRIA F, BARON-WIECHEC A, SKELDON P, THOMPSON G E. Study of the formation of alkaline electroless Ni−P coating on magnesium and AZ31B magnesium alloy [J]. Surface and Coatings Technology, 2017, 321: 309−320.
[30] WU L, YANG Z, QIN G. Kinetic study of a novel electroless NiP deposition on AZ91D magnesium alloy using nickel hypophosphite as the metal salt [J]. Journal of Alloys and Compounds, 2017, 694: 1133−1139.
[31] EL-TAIB HEAKAL F, SHOEIB M A, MAANOUM M A. Optimizing parameters affecting electroless Ni−P coatings on AZ91D magnesium alloy as corrosion protection barriers [J]. Protection of Metals and Physical Chemistry of Surfaces, 2017, 53: 177−187.
[32] SEIFZADEH D, KAZEMI MOHSENABADI H. Corrosion protection of AM60B magnesium alloy by application of electroless nickel coating via a new chrome-free pretreatment [J]. Bulletin of Materials Science, 2017, 40: 407−415.
[33] RAJABALIZADEH Z, SEIFZADEH D. The effect of copper ion on microstructure, plating rate and anticorrosive performance of electroless Ni−P coating on AZ61 magnesium alloy [J]. Protection of Metals and Physical Chemistry of Surfaces, 2014, 50: 516−523.
[34] BRETT C M A, BRETT A M O. Electrochemistry: Principles, methods, and applications [M]. Oxford: Oxford University Press, 1994.
[35] ZENG R C, SUN L, ZHENG Y F, CUI H Z, HAN E H. Corrosion and characterisation of dual phase Mg−Li−Ca alloy in Hank's solution: The influence of microstructural features [J]. Corrosion Science, 2014, 79: 69−82.
[36] HU J, FANG L, LIAO X L, SHI L T. Influences of different reinforcement particles on performances of electroless composites [J]. Surface Engineering, 2017, 33: 362−368.
[37] LIU H, BI S, CAO L, BAI Q, TENG X, YU Y. The deposition process and the properties of direct electroless nickel–phosphorous coating with chromium-free phosphate pickling pretreatment on AZ31 magnesium alloy [J]. International Journal of Electrochemical Science, 2012, 7: 8337−8355.
[38] JIANG B, JIANG S L, MA A L, ZHENG Y G. Effect of heat treatment on erosion–corrosion behavior of electroless Ni−P coatings in saline water [J]. Materials and Manufacturing Processes, 2014, 29: 74−82.
[39] SEIFZADEH D, FARHOUDI L. Electroless Co−P plating on magnesium alloy and its anti-corrosion properties [J]. Surface Engineering, 2016, 32: 348−355.
[40] NEZAMDOUST S, SEIFZADEH D. Application of Ce−V/sol–gel composite coating for corrosion protection of AM60B magnesium alloy [J]. Transactions of Nonferrous Metals Society of China, 2017, 27: 352−362.
[41] CURIONI M. The behaviour of magnesium during free corrosion and potentiodynamic polarization investigated by real-time hydrogen measurement and optical imaging [J]. Electrochimica Acta, 2014, 120: 284−292.
[42] SONG Y W, SHAN D Y, HAN E H. Comparative study on corrosion protection properties of electroless Ni−P−ZrO_2 and Ni−P coatings on AZ91D magnesium alloy [J]. Materials and Corrosion, 2007, 58: 506−510.

低温制备镁合金无预处理 Ni−P 涂层

P. SHOGHI, D. SEIFZADEH, M. GHOLIZADEH-GHESHLAGHI, A. HABIBI-YANGJEH

Applied Chemistry Department, University of Mohaghegh Ardabili, Ardabil, Iran

摘　要：在低温下用电化学促进化学镀(EPEP)在 AM60B 镁合金上制备无预处理 Ni−P 涂层，并用 SEM、AFM、EDS 和 XRD 等技术对涂层进行表征。在阴极电流密度为 4 mA/cm^2、温度为 50 °C 的条件下获得致密、均匀和中等磷含量的 Ni−P 涂层，其显微组织为晶态−无定型的混合态。在相同的化学镀条件下，但不施加阴极电流，合金表面形成了岛状的镍团簇镀层。在 3.5% NaCl 腐蚀电解液中进行电化学检测，发现 EPEP 镀后镁合金的耐蚀性有了明显提高。显微电镜观察进一步证实了电化学测试的结果，涂层的厚度、显微硬度、孔隙度及粘结强度均合格。

关键词：镁合金；腐蚀；低温化学镀；N−P 涂层

(Edited by Wei-ping CHEN)